

# Threshold $\pi^-$ Photoproduction on the Neutron

W. J. Briscoe,<sup>1</sup> A. E. Kudryavtsev,<sup>2,1</sup> I. I. Strakovsky,<sup>1,\*</sup> V. E. Tarasov,<sup>2</sup> and R. L. Workman<sup>1</sup>

<sup>1</sup>*Institute for Nuclear Studies, Department of Physics,  
The George Washington University, Washington DC 20052, USA*

<sup>2</sup>*National Research Centre “Kurchatov Institute”,  
Institute for Theoretical and Experimental Physics (ITEP), Moscow 117218, Russia*  
(Dated: November 22, 2021)

Recent data from the PIONS@MAX-lab Collaboration, measuring the total cross section of the pion incoherent photoproduction  $\gamma d \rightarrow \pi^- pp$  near threshold, have been used to extract the  $E_{0+}$  multipole and total cross section of the reaction  $\gamma n \rightarrow \pi^- p$ , also near threshold. These are the first measurements of the reaction  $\gamma d \rightarrow \pi^- pp$  in the threshold region. The value of  $E_{0+}$  is extracted through a fit to the deuteron data in a photoproduction model accounting for final-state interactions. The model takes an  $S$ -wave approximation for the elementary reaction  $\gamma n \rightarrow \pi^- p$  with  $E_{0+} = \text{const}$  in the threshold region. The obtained value  $E_{0+} = -31.86 \pm 0.8$  (in  $10^{-3}/m_{\pi^+}$  units) is in agreement with other existing results. Model predictions for the total cross section  $\sigma(\gamma n \rightarrow \pi^- p)$  are also given.

## I. INTRODUCTION

Pion photoproduction measurements facilitate the understanding of the strong force in the low-energy regime. However, most of the experimental efforts over the last few decades have focused on neutral pion production from proton targets  $\gamma p \rightarrow \pi^0 p$  [1]. Incoherent pion photoproduction on the deuteron is interesting in that it provides information on the elementary reaction from a neutron target, i.e.,  $\gamma n \rightarrow \pi N$ . Generally, these latter data are poorly determined due to the paucity of neutron reaction data.

A theory of pion photoproduction was constructed in the 1950’s. Kroll and Ruderman [2] were the first to derive model-independent predictions in the threshold region, a so-called Low Energy Theorem (LET), by applying gauge and Lorentz invariance to the reaction  $\gamma N \rightarrow \pi N$ . The general formalism for this process was developed by Chew and co-workers [3] (CGLN amplitudes). Vainshtein and Zakharov extended the LET by including the hypothesis of a Partially Converted Axial Current (PCAC) [4]. The derivation of the theorem is based on the use of the PCAC hypothesis and on the expansion of the amplitudes in powers of  $k/m_{int}$  and  $q/m_{int}$ , where  $k$  and  $q$  are pion and photon four-momenta and  $m_{int}$  is some internal mass. This work succeeded in describing the threshold amplitude as a power series in the ratio  $\chi = m_{\pi}/m$  up to terms of order  $\chi^2$  ( $m_{\pi}$  and  $m$  are the averaged pion and nucleon masses). Somewhat later, Berends and co-workers [5] analysed the existing data in terms of a multipole decomposition and extracted the various multipole amplitudes contributing in a region up to an excitation energy of 500 MeV. These amplitudes are vital inputs to low-energy descriptions of hadron physics based on the Chiral Perturbation Theory ( $\chi$ PT) [6].

Measurements of pion photoproduction on both proton and “neutron” targets have a very long history, dating

back about 70 years, involving by the University of Bristol group [7]. The first bremsstrahlung facilities produced pioneering results for  $\gamma p \rightarrow \pi^+ n$  [8] and  $\gamma p \rightarrow \pi^0 p$  [9]. It is impressive that this work started two years after the pion discovery in 1947 [10]. The first  $\gamma n \rightarrow \pi^- p$  photoproduction experiment used the 318-MeV photon beam from the Berkeley electron synchrotron and a high pressure, low temperature deuterium target [11]. Despite all the shortcomings of the first measurements (such as large normalization uncertainties, wide energy and angular binning, limited angular coverage, etc.), those measurements were crucial for the discovery of the first baryon resonance,  $\Delta$ -isobar [12].

Present experimental facilities allow some of the most challenging problems of intermediate energy physics to be studied. These include the behavior of charged and neutral pion production at threshold and the electric quadrupole amplitude,  $E_0^+$ . Threshold measurements of  $\pi^0$  photoproduction, from a proton target, have been obtained with greater kinematic coverage and higher precision than the associated charged pion photoproduction channels (Table I).

TABLE I. Threshold energies for pion photoproduction and number of measurements at the threshold (below  $E_{\gamma} = 180$  MeV) as available in GWU SAID database [13].

Reaction	W (MeV)	E (MeV)	$d\sigma/d\Omega$	Pol
$\gamma p \rightarrow \pi^0 p$	1073.2	144.7	1110	508
$\gamma n \rightarrow \pi^0 n$	1074.5	144.7	0	0
$\gamma n \rightarrow \pi^- p$	1077.8	148.4	21	12
$\gamma p \rightarrow \pi^+ n$	1079.1	151.4	112	0

The total cross section at the pion production threshold is known for  $\gamma p \rightarrow \pi^0 p$  while information about other pion photoproduction reactions comes mainly through an extrapolation of partial-wave analyses (PWA), such as SAID [14] and MAID [15], and does not have experimental confirmation

\* Corresponding author; igor@gwu.edu

(Fig. 1) .

Recently, the PIONS@MAX-lab Collaboration has reported total cross section measurements of the pion incoherent photoproduction  $\gamma d \rightarrow \pi^- pp$  at threshold [16]. The experiment was performed at the Tagged-Photon Facility [17] at the MAX IV Laboratory in Lund, Sweden [18]. Data were collected by three very large NaI(Tl) spectrometers BUNI, CATS, and DIANA. The measured total cross section of the reaction  $\gamma d \rightarrow \pi^- pp$  and the comparison with our theoretical predictions was shown in Fig. 5 of Ref. [16].

The present paper is focused on a determination of the total cross sections for  $\pi^-$  photoproduction on a “neutron” target,  $\gamma n \rightarrow \pi^- p$ , utilizing the deuteron measurements, where model-dependent nuclear (final-state interaction) (FSI) corrections play a critical role.

## II. THEORETICAL ANALYSIS

### A. Extraction of the $\gamma n \rightarrow \pi^- p$ Cross Sections

A mathematical description of the FSI model is given in Appendix. Here the features of this model are summarized. Compared to the elementary reaction  $\gamma n \rightarrow \pi^- p$ , the additional FSI treatment has a non-negligible effect on the cross section. The full model [19] is applied with simplifications corresponding to the near-threshold region. The four diagrams in Fig. 2 are calculated, where  $M_a$  is the Impulse Approximation (IA) term;  $M_b$  and  $M_c$  are the  $NN$  and  $\pi N$  FSI terms;  $M_d$  is the  $NN$ -FSI term with pion rescattering in the intermediate state (the “two-loop” term added here). Both  $M_a$  and  $M_c$  are the sums of two terms, arising from permutation of the final protons. The total amplitude  $M_{\gamma d}$  is taken as the sum  $M_{\gamma d} = M_a + M_b + M_c + M_d$ .

General expressions for the total cross sections of the reactions of interest can be written as

$$\begin{aligned} \sigma(\gamma n \rightarrow \pi^- p) &= 4\pi \frac{k}{q_{\gamma n}} \overline{|F_{\gamma n}|^2}, \\ \sigma(\gamma d \rightarrow \pi^- pp) &= \frac{1}{4q_{\gamma d}\sqrt{s}} \int \overline{|M_{\gamma d}|^2} d\tau_3. \end{aligned} \quad (1)$$

Here:  $q_{\gamma n}(k)$  and  $\overline{|F_{\gamma n}|^2}$  are the center-of-mass (CM) momentum of the initial photon (final pion) in the reaction  $\gamma n \rightarrow \pi^- p$ , and the amplitude squared (unpolarized case);  $q_{\gamma d}$  and  $\sqrt{s}$  are the the CM momentum of the initial photon and total energy in the reaction  $\gamma d \rightarrow \pi^- pp$ ;  $\overline{|M_{\gamma d}|^2}$  and  $d\tau_3$  are the invariant amplitude squared of the reaction  $\gamma d \rightarrow \pi^- pp$  (unpolarized case) and phase-space element of the final  $\pi^- pp$  system, where

$$\begin{aligned} d\tau_3 &= I \frac{Qp dw dz_1 d\varphi_1}{2\pi(4\pi)^3 \sqrt{s}}, \quad p = \sqrt{2\mu w}, \\ Q &= \sqrt{2\bar{m}(E^* - w)}, \quad w = M_{pp} - 2m_p. \end{aligned} \quad (2)$$

Here:  $I = 1/2$  is the symmetry factor for two identical protons;  $E^* = \sqrt{s} - \mu - 2m_p$  is the excess energy;  $\mu(m_p)$

is the  $\pi^-$  (proton) mass;  $m = (m_p + m_n)/2$ ;  $M_{pp}$  is the effective mass of the  $pp$  system;  $\bar{m} = 2m\mu/(2m + \mu)$ ,  $\bar{\mu} = m\mu/(m + \mu)$ ;  $z = \cos\theta$ ,  $z_1 = \cos\theta_1$ ;  $\theta$  is the  $\pi^-$  polar angle in the reaction rest frame;  $\theta_1$  and  $\varphi_1$  are the polar and azimuthal angles of relative motion in the  $pp$  system. All the kinematical variables, needed to calculate the amplitude  $\overline{|M_{\gamma d}|^2}$ , can be expressed through  $E^*$ ,  $w$ ,  $z$ ,  $z_1$ , and  $\varphi_1$ .

The ingredients and approximations, used here in the model, are as follows.

1) In the threshold region, we use the  $s$ -wave  $\gamma n \rightarrow \pi^- p$  amplitude, given by the  $E_{0+}$  multipole, taken to be constant. We include only the charged intermediate pion  $\pi^-$  in the diagrams  $M_c$  and  $M_d$  since the contribution of intermediate  $\pi^0$  is suppressed due to a small photoproduction  $\gamma N \rightarrow \pi^0 N$  amplitudes. Thus,  $F_{\gamma n} = E_{0+}$  and  $M_{\gamma d} \sim E_{0+}$ . Hereafter  $E_{0+} \equiv E_{0+}(\gamma n \rightarrow \pi^- p)$ . In this approximation,  $\sigma(\gamma n \rightarrow \pi^- p) \sim E_{0+}^2$  and

$$\sigma(\gamma d \rightarrow \pi^- pp) = E_{0+}^2 \sigma_0, \quad (3)$$

where  $\sigma_0$  is  $\sigma(\gamma d \rightarrow \pi^- pp)$ , calculated according to Eq. (1) with the factor  $E_{0+}$  taken out of the amplitude  $M_{\gamma d}$ , i.e.,  $\sigma_0$  doesn't depend on  $E_{0+}$ .

2) In the  $NN$ -FSI ( $M_b$ ) and 2-loop ( $M_d$ ) terms, the  $S$ -wave  $pp$ -scattering amplitude, which also includes the Coulomb effects, was taken from Ref. [20]. The off-shell correction to the  $pp$  amplitude was taken into account as was done previously, in Refs. [19, 21], by multiplying the on-shell  $pp$  amplitude by the monopole form factor  $F(q, p) = (p^2 + \beta^2)/(q^2 + \beta^2)$ . Here:  $q$  and  $p$  are the relative momenta of the intermediate and final protons;  $\beta = 1.2$  fm.

3) In the  $\pi N$ -FSI ( $M_c$ ) and 2-loop ( $M_d$ ) terms, the  $S$ -wave  $\pi^- p$ -scattering amplitude  $a_{\pi^- p} = b_0 - b_1$  is used, fixed by the isospin scattering lengths  $b_0 = -28$  and  $b_1 = -881$  in  $10^{-4}/\mu$  units [22].

4) The deuteron wave function (DWF) of the Bonn potential was used in parametrization from Ref. [23]. Both  $S$ - and  $D$ -wave parts of DWF are included in the IA diagram  $M_a$ , while  $D$ -wave part is neglected in the diagrams  $M_b$ ,  $M_c$ , and  $M_d$ .

The terms  $M_{a,b,c,d}$  and the total amplitude squared,  $\overline{|M_{\gamma d}|^2}$  (unpolarized case), are written out in Appendix (Sections 1 and 2). In the given approximation, the integrals over the intermediate states in the loop terms  $M_{b,c,d}$  are obtained in analytic form (see Appendix, Section 3).

Now we fit the latest data by the PIONS@MAX-lab Collaboration [16] on  $\sigma^{exp}(\gamma d \rightarrow \pi^- pp)$  close to threshold by the Eq. (3), making use of  $E_{0+}$  as a free parameter, and obtain  $E_{0+}(1-6) = -31.86 \pm 0.8$  (in  $10^{-3}/\mu$  units). The notation (1-6) means that the  $\chi^2$  fit includes all the 6 data points in Fig. 3. The curves show the cross sections, calculated according to Eq. (3), where the red solid one shows the result obtained with the total amplitude  $M_{\gamma d}$ . The other curves are explained in the figure caption. One can see that the main effect of

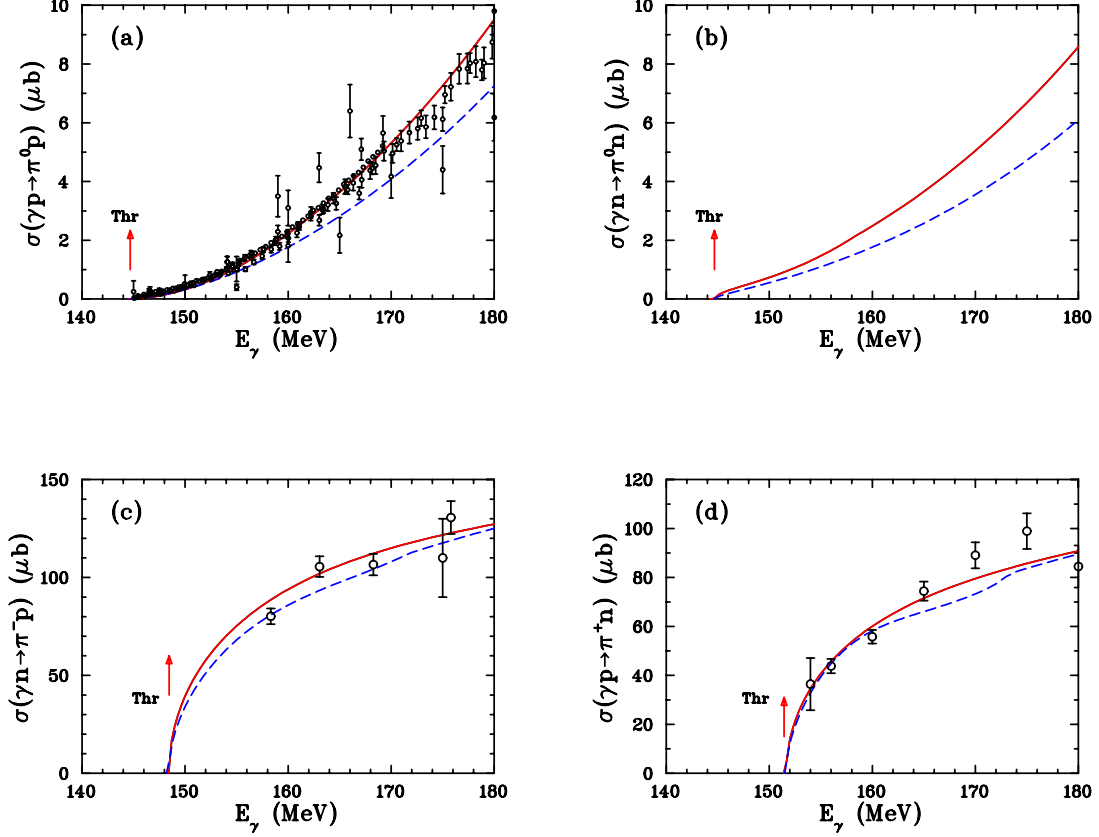


FIG. 1. Total cross section of the reactions  $\gamma p \rightarrow \pi^0 p$  (a),  $\gamma n \rightarrow \pi^0 n$  (b),  $\gamma n \rightarrow \pi^- p$  (c), and  $\gamma p \rightarrow \pi^+ n$  (d). Open black circles are the previous measurements [13]. Plotted uncertainties are statistical and systematic in quadrature. Red solid (blue dashed) curves are predictions by the SAID MA19 [14] (MAID2007 [15]) solution. Both solutions did not use new MAX-lab data in fits.

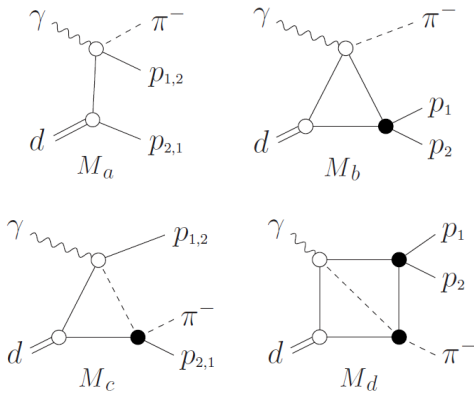


FIG. 2. The IA ( $M_a$ ), NN-FSI ( $M_b$ ),  $\pi N$ -FSI ( $M_c$ ), and 2-loop ( $M_d$ ) diagrams for the reaction  $\gamma d \rightarrow \pi^- pp$ .

FSI comes from the NN-FSI term  $M_b$  (compare magenta dash-dotted, blue long dashed curves in Fig. 3), while the role of the terms  $M_c$  and  $M_d$  is small.

A relatively large disagreement of the model with the data is observed close to threshold at  $E_\gamma = 147$  MeV. Excluding this “bad” 1-st data point from the fit, we obtain  $E_{0+}(2-6) = -31.75 \pm 0.8$  (the same units). Both variants, (1–6) and (2–6), are in agreement with the value  $E_{0+} = -31.9$  from Ref. [24]. The model also overestimates the data above  $E_\gamma \sim 156$  MeV. If one excludes two data points (5-th and 6-th) at  $E_\gamma = 157.6$  MeV and 159.8 MeV in Fig. 3, then the  $\chi^2$  fit gives  $E_{0+}(1-4) = -33.70 \pm 1.2$  and  $E_{0+}(2-4) = -33.94 \pm 1.2$ . Suppose this discrepancy partly comes from the model approximations with energy-independent  $\gamma n \rightarrow \pi^- p$  amplitude  $E_{0+} = \text{const}$ . Let us briefly discuss the effects not included here, connected with energy dependence of  $E_{0+}$  and  $P$ -wave contribution to the  $\gamma n \rightarrow \pi^- p$  amplitude. We can roughly estimate these corrections from the results of Ref. [25] on the reaction  $\gamma d \rightarrow \pi^+ nn$  in the chiral perturbation theory, where the Born  $\gamma n \rightarrow \pi^- p$  amplitudes (with a Kroll-Ruderman term) in the threshold region were used. At  $\Delta E_\gamma = E_\gamma - E_{th} = 15$  MeV ( $E_{th}$  is the threshold energy), the energy-dependent correction

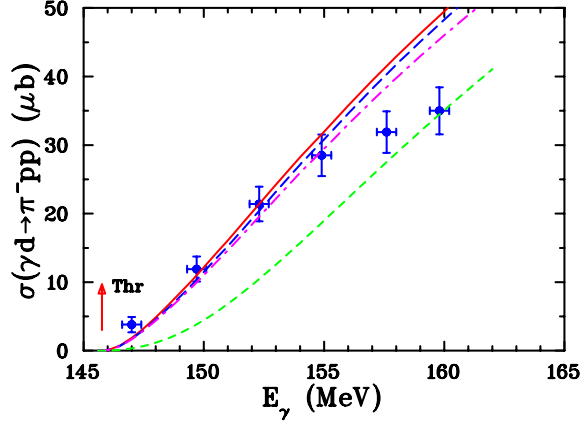


FIG. 3. Total cross section of the reaction  $\gamma d \rightarrow \pi^- pp$ : blue filled circles are the MAX-lab data [16];  $E_\gamma$  is the photon energy in the laboratory frame; the statistical and systematic uncertainties from Table II of Ref. [16] are summed in quadrature. Green short dashed curve shows the result, obtained with the IA amplitude  $M_a$  in Fig. 2. Successive addition of  $M_b(NN\text{-FSI})$ ,  $M_c(\pi N\text{-FSI})$  and  $M_d(2\text{-loop})$  terms leads to magenta dash-dotted, blue long dashed, and red solid curves, respectively.

to the constant  $E_{0+}$  decreases the total cross sections by  $\sim 6\%$  (Fig. 8 of Ref. [25]), while the  $P$ -wave contribution increases it by  $\sim 3\%$  (Fig. 9 there). Approximately the same corrections for the reaction  $\gamma d \rightarrow \pi^- pp$  seem not enough to improve essentially the discrepancy in Fig. 3 above  $E_\gamma \sim 156$  MeV. We leave these details for a future study.

Table II shows the cross sections  $\sigma(\gamma n \rightarrow \pi^- p)$  from Eq. (1) at  $F_{\gamma n} = E_{0+}(1-6) = -31.86 \pm 0.8$ . The results are given at the same values  $\Delta E_\gamma = E_\gamma - E_{th}$  as in Fig. 3, i.e., the  $E_\gamma$ 's are shifted by the difference  $(148.44 - 145.76)$  MeV of the  $\gamma n \rightarrow \pi^- p$  and  $\gamma d \rightarrow \pi^- pp$  threshold energies. Total uncertainties included statistical and systematical uncertainties of the MAX-lab experimental data with the FSI contribution.

As an aside, we have previously used this GW-ITEP FSI code to determine, at much higher energies, the  $\gamma n \rightarrow \pi^- p$  differential cross section from  $\gamma d \rightarrow \pi^- pp$  measurements with CLAS and A2 at MAMI Collaborations [14, 19, 26–28]. In this way, we succeeded in the first determination of neutron couplings at a set of pole positions [14, 28] using these additions to the world data.

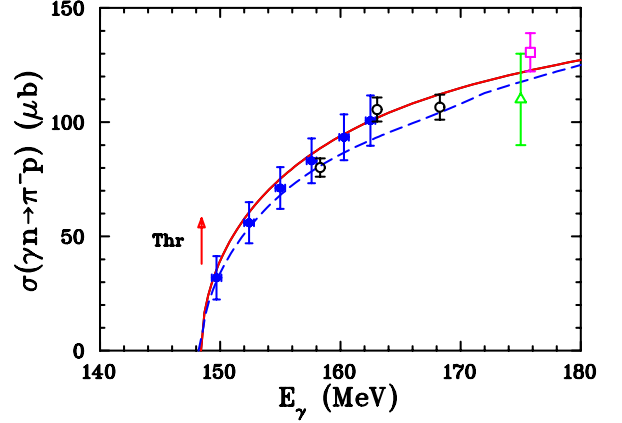


FIG. 4. Total cross section of the reaction  $\gamma n \rightarrow \pi^- p$ . Previous measurements for the inverse reaction  $\pi^- p \rightarrow \gamma n$  are from Cornell synchrotron [30] (green open triangle), and TRIUMF [31] (magenta open square) and [32] (black open circles). Statistical and systematical uncertainties are summed in quadrature. Red solid (blue dashed) curves are predictions by the SAID MA19 [14] (MAID2007 [15]) solution.

TABLE II. Total cross section for  $\pi^-$  photoproduction on the neutron with statistical and systematic uncertainties in quadratures.

$E_\gamma$ (MeV)	$\sigma$ ( $\mu\text{b}$ )	Exp Stat	Exp Sys	$E_{0+}$ fit Sys
$149.7 \pm 0.4$	$31.9 \pm 9.5$	5.3	28.9	4.9
$152.4 \pm 0.4$	$56.0 \pm 9.0$	2.5	15.1	4.9
$155.0 \pm 0.4$	$71.2 \pm 9.1$	1.4	11.7	4.9
$157.6 \pm 0.4$	$83.1 \pm 9.8$	1.8	10.5	4.9
$160.3 \pm 0.4$	$93.4 \pm 10.0$	1.3	9.4	4.9
$162.5 \pm 0.4$	$100.7 \pm 11.0$	1.4	9.7	4.9

## B. Summary and Impact of new MAX-lab data for Partial-Wave Analysis

In summary, total cross sections for the  $\gamma n \rightarrow \pi^- p$  have been taken at photon energies within 1-2 MeV of the reaction threshold. These data are in good agreement with predictions from previous analyses, such as SAID and MAID.

In general, to prevent double counting, we do not use total cross section data (integral over differential cross sections) in the SAID partial-wave analyses. Specifically at the threshold, it is hard to cover a full angular range and some assumptions are required to determine a total cross section.

The importance of improving the  $\gamma n$  database relative to the  $\gamma p$  database is directly related to the fact that the electromagnetic interaction does not conserve isospin

symmetry. The amplitude for the reactions  $\gamma N \rightarrow \pi N$  factors into distinct  $I = 1/2$  and  $I = 3/2$  isospin components,  $A_{\gamma, \pi^\pm} = \sqrt{2}(A_{p/n}^{I=1/2} \mp A^{I=3/2})$  (see Ref. [24]). This expression indicates that the  $I = 3/2$  multipoles can be entirely determined from proton target data. However, measurements from datasets with both neutron and proton targets are required to determine the isospin  $I = 1/2$  amplitudes.

### III. ACKNOWLEDGEMENTS

This work was supported in part by the U.S. Department of Energy, Office of Science, Office of Nuclear Physics under Awards No. DE-SC0016583 and DE-SC0016582. The authors A.E.K. and V.E.T. acknowledge the support of the RFBR under Award No. 16-02-00767.

### APPENDIX: THE REACTION AMPLITUDE

#### 1. The Reaction Amplitude

The invariant amplitude  $M_{\gamma d}$  of the reaction  $\gamma d \rightarrow \pi^- pp$  can be written as

$$\begin{aligned} M_{\gamma d} &= c\varphi_1^+(L + i\mathbf{K} \cdot \boldsymbol{\sigma})\varphi_2^c, \\ c &= 16\pi W\sqrt{m} \quad (W = m + \mu), \\ L &= L_a + L_b + L_c + L_d, \\ L_a &= L_a^{(s)} + L_a^{(d)}, \\ \mathbf{K} &= \mathbf{K}_a + \mathbf{K}_b + \mathbf{K}_c + \mathbf{K}_d, \\ \mathbf{K}_a &= \mathbf{K}_a^{(s)} + \mathbf{K}_a^{(d)}. \end{aligned} \quad (A.1)$$

Here:  $\varphi_{1,2}$  are the spinors of the final protons ( $\varphi^+ \varphi \equiv 1$ ) and  $\varphi^c \equiv \sigma_2 \varphi^*$ ; the subscripts  $a, b, c, d$  (in  $L_a, \dots, \mathbf{K}_a, \dots$ ) correspond to the diagrams in Fig. 2;  $L_a^{(s)}$  and  $\mathbf{K}_a^{(s)}$  ( $L_a^{(d)}$  and  $\mathbf{K}_a^{(d)}$ ) are the IA amplitudes with  $s$ -wave ( $d$ -wave) part of the DWF. The amplitudes  $L_a, \dots$  and  $\mathbf{K}_a, \dots$  are given below, where  $\mathbf{e}$  and  $\boldsymbol{\epsilon}$  are the photon and deuteron polarization three-vectors, respectively. Hereafter:  $\mathbf{q}, \mathbf{k}, \mathbf{p}_{1,2}$  stand for the three-momenta of the initial photon, final pion and final protons, respectively, in the laboratory frame.

#### a) IA Terms:

$$\begin{aligned} L_a^{(s)} &= x_a E_{0+}(\mathbf{e} \cdot \boldsymbol{\epsilon}), \quad x_a = f_1 + f_2, \\ L_a^{(d)} &= -\left[ g_1(\mathbf{e} \cdot \mathbf{n}_1)(\mathbf{e} \cdot \mathbf{n}_2) + \right. \\ &\quad \left. + g_2(\mathbf{e} \cdot \mathbf{n}_2)(\boldsymbol{\epsilon} \cdot \mathbf{n}_1) \right] E_{0+}, \\ \mathbf{K}_a^{(s)} &= y_a E_{0+}[\mathbf{e} \times \boldsymbol{\epsilon}], \quad y_a = f_2 - f_1, \\ \mathbf{K}_a^{(d)} &= \left( g_2(\boldsymbol{\epsilon} \cdot \mathbf{n}_2)[\mathbf{n}_2 \times \mathbf{e}] - \right. \\ &\quad \left. - g_1(\boldsymbol{\epsilon} \cdot \mathbf{n}_1)[\mathbf{n}_1 \times \mathbf{e}] \right) E_{0+}; \\ f_{1,2} &= \frac{u(p_{1,2})}{\sqrt{2}} + \frac{w(p_{1,2})}{2}, \\ g_{1,2} &= \frac{3}{2} w(p_{1,2}), \quad \mathbf{n}_{1,2} = \frac{\mathbf{p}_{1,2}}{p_{1,2}}. \end{aligned} \quad (A.2)$$

Here:  $\mathbf{n}_{1,2}$  – the unit vectors;  $u(p)$  and  $w(p)$  are the  $S$ - and  $D$ -wave parts of the DWF. We use DWF [23], parametrized in the form

$$u(p) = \sum_j \frac{C_j}{p^2 + m_j^2}, \quad w(p) = \sum_j \frac{D_j}{p^2 + m_j^2} \quad (A.3)$$

with normalization  $\int d\mathbf{p} [u^2(p) + w^2(p)] = (2\pi)^3$ .

#### b) $pp$ -FSI Terms:

$$\begin{aligned} L_b &= x_b E_{0+}(\mathbf{e} \cdot \boldsymbol{\epsilon}), \quad \mathbf{K}_b = 0, \\ x_b &= 2I_{pp}(p, \beta, \Delta) f_{pp}(p), \\ I_{pp}(p, \beta, \Delta) &= \int \frac{d\mathbf{x} f(x, p) u(|\mathbf{x} + \boldsymbol{\Delta}|)}{2\pi^2 \sqrt{2} (x^2 - p^2 - i0)}, \\ f(x, p) &= \frac{p^2 + \beta^2}{x^2 + \beta^2}, \quad \boldsymbol{\Delta} = \frac{1}{2}(\mathbf{p}_1 + \mathbf{p}_2). \end{aligned} \quad (A.4)$$

Here:  $f_{pp}(p)$  is the on-shell  $S$ -wave  $pp$ -scattering amplitude in the Effective-Range-Approximation with Coulomb effects included [20];  $\mathbf{x}$  is the relative three-momentum of the intermediate nucleons;  $f(x, p)$  is the formfactor in the off-shell  $pp$ -scattering amplitude  $f_{pp}^{off}(x, p) = f(x, p) f_{pp}(p)$  with parameter  $\beta = 1.2$  fm, used earlier [19, 21]. The integral  $I_{pp}(p, \beta, \Delta)$  is written out in Eqs. (A.9) and (A.10).

#### c) $\pi N$ -FSI Terms:

$$\begin{aligned} L_c &= x_c E_{0+} a_{\pi^- p}(\mathbf{e} \cdot \boldsymbol{\epsilon}), \quad x_c = I_1 + I_2; \\ \mathbf{K}_c &= y_c E_{0+} a_{\pi^- p}[\mathbf{e} \times \boldsymbol{\epsilon}], \quad y_c = I_1 - I_2; \\ I_i &= I(k_i^2, \Delta_i), \quad \Delta_i = \frac{m}{m + \mu}(\mathbf{k} + \mathbf{p}_i). \end{aligned} \quad (A.5)$$

Here:  $k_i$  are the relative momenta in the pion-proton pairs  $\pi^- p_i$  ( $i = 1, 2$ );  $a_{\pi^- p}$  is the  $\pi^- p$ -scattering amplitude in the scattering-length approximation (see the main text). The integral  $I(k_{1,2}^2, \Delta_{1,2})$  is written out below in Eq. (A.9).

d) 2-loop Terms:

$$\begin{aligned}
L_d &= x_d E_{0+} (\mathbf{e} \cdot \boldsymbol{\epsilon}), \quad \mathbf{K}_d = 0, \\
x_d &= 2K(p, b, \Delta) f_{pp}(p) a_{\pi-p}, \\
K(p, b, \Delta) &= \frac{m+\mu}{m} \times \\
&\times \int \frac{d\mathbf{x} d\mathbf{y} u(|\mathbf{x}+\mathbf{y}-\Delta|) f(x, p)}{4\pi^4 \sqrt{2} (x^2 - p^2 - i0)(y^2 - b^2 - i0)}, \\
\Delta &= \frac{1}{2}(\mathbf{q} + \mathbf{k}), \quad b^2 = 2\mu(\sqrt{s} - \sqrt{s_0}) \geq 0.
\end{aligned} \tag{A.6}$$

Here:  $\sqrt{s_0} = 2m_p + \mu$ ;  $f(x, p)$  is given in Eq. (A.4); the denominator  $(y^2 - b^2 - i0)$  of the pion propagator is obtained, neglecting the kinetic energies (static approximation) of the intermediate nucleons. The expression for  $K(p, b, \Delta)$  is given in Eqs. (A.11) and (A.12).

## 2. The Square of the Amplitude

The square of the amplitude (A.1) for unpolarized nucleons is  $|M_{\gamma d}|^2 = 2c^2 (|L|^2 + |\mathbf{K}|^2)$ . Averaging it over the photon and deuteron polarization states, we write

$$\overline{|M_{\gamma d}|^2} = 2c^2 (\overline{|L|^2} + \overline{|\mathbf{K}|^2}). \tag{A.7}$$

Making use of Eqs. (A.2), (A.4), (A.5), and (A.6), we have

$$\begin{aligned}
L &= A E_{0+} (\mathbf{e} \cdot \boldsymbol{\epsilon}) + L_a^{(d)}, \quad A = x_a + x_b + x_c + x_d, \\
\mathbf{K} &= B E_{0+} [\mathbf{e} \times \boldsymbol{\epsilon}] + \mathbf{K}_a^{(d)}, \quad B = y_a + y_c.
\end{aligned}$$

Then, we obtain

$$\begin{aligned}
\overline{|L|^2} &= \frac{1}{3} \left[ |A|^2 - (g_1 n_{1t}^2 + g_2 n_{2t}^2) \text{Re}[A] + \right. \\
&\quad \left. + \frac{1}{2} (g_1^2 n_{1t}^2 + g_2^2 n_{2t}^2) \right. \\
&\quad \left. + g_1 g_2 (\mathbf{n}_1 \cdot \mathbf{n}_2) (\mathbf{n}_{1t} \cdot \mathbf{n}_{2t}) \right] E_{0+}^2, \\
\overline{|\mathbf{K}|^2} &= \frac{1}{3} \left[ 2|B|^2 + \right. \\
&\quad \left. + [g_1(1 + n_{1z}^2) - g_2(1 + n_{2z}^2)] \text{Re}[B] + \right. \\
&\quad \left. + \frac{1}{2} [g_1^2(1 + n_{1z}^2) + g_2^2(1 + n_{2z}^2)] - \right. \\
&\quad \left. - g_1 g_2 (\mathbf{n}_1 \cdot \mathbf{n}_2) [(\mathbf{n}_1 \cdot \mathbf{n}_2) + n_{1z} n_{2z}] \right] E_{0+}^2.
\end{aligned} \tag{A.8}$$

Here:  $\mathbf{n}_{1t,2t}$  and  $n_{1z,2z}$  are, respectively, the transverse

parts and  $z$ -components of the unit vectors  $\mathbf{n}_{1,2}$ , defined in Eqs. (A.2), with  $z$ -axis along the photon three-momentum  $\mathbf{q}$  in the laboratory frame.

## 3. The Integrals

The integral  $I_{pp}(p, \beta, \Delta)$  in Eqs. (A.4) can be rewritten as

$$\begin{aligned}
I_{pp}(p, \beta, \Delta) &= I(p^2, \Delta) - I(-\beta^2, \Delta), \\
I(a^2, \Delta) &= \int \frac{d\mathbf{x} u(|\mathbf{x} + \Delta|)}{2\pi^2 \sqrt{2} (x^2 - a^2 - i0)}.
\end{aligned} \tag{A.9}$$

For the DWF, given in the form (A.3), we obtain

$$\begin{aligned}
I(a^2 > 0, \Delta) &= \sum_j \frac{C_j}{2\Delta\sqrt{2}} \left[ \arctan \frac{|a| + \Delta}{m_j} - \right. \\
&\quad \left. - \arctan \frac{|a| - \Delta}{m_j} + \frac{i}{2} \ln \frac{m_j^2 + (|a| + \Delta)^2}{m_j^2 + (|a| - \Delta)^2} \right], \\
I(a^2 < 0, \Delta) &= \sum_j \frac{C_j}{\Delta\sqrt{2}} \arctan \frac{\Delta}{m_j + |a|}.
\end{aligned} \tag{A.10}$$

The integral  $K(p, b, \Delta)$  in Eqs. (A.6) can be written as

$$\begin{aligned}
K(p, b, \Delta) &= K_0(p^2, b^2, \Delta) - K_0(-\beta^2, b^2, \Delta), \\
K_0(a^2, b^2, \Delta) &= \frac{m+\mu}{m} \times \\
&\times \int \frac{d\mathbf{x} d\mathbf{y} u(|\mathbf{x} + \mathbf{y} - \Delta|)}{4\pi^4 \sqrt{2} (x^2 - a^2 - i0)(y^2 - b^2 - i0)},
\end{aligned} \tag{A.11}$$

For the DWF of the type (A.3), we obtain

$$\begin{aligned}
K_0(a^2, b^2, \Delta) &= \sum_j \frac{C_j}{\Delta\sqrt{2}} \left[ U_j(a^2, b^2, \Delta) - \right. \\
&\quad \left. - U_j(a^2, b^2, -\Delta) \right], \\
U_j(a^2, b^2, \Delta) &= -x_j A_j - y L_j + \\
&\quad + i(y A_j - x_j L_j), \\
L_j &= \frac{1}{2} \ln(x_j^2 + y^2), \quad A_j = \arctan \frac{y}{x_j}; \\
a^2 > 0: \quad x_j &= m_j, \quad y = |a| + |b| + \Delta; \\
a^2 < 0: \quad x_j &= m_j + |a|, \quad y = |b| + \Delta.
\end{aligned} \tag{A.12}$$

- 
- [1] D. G. Ireland, E. Pasyuk, and I. Strakovsky, Prog. Part. Nucl. Phys. **111**, 103752 (2020).  
[2] N. M. Kroll and M. A. Ruderman, Phys. Rev. **93**, 233 (1954).  
[3] G. F. Chew, M. L. Goldberger, F. E. Low, and Y. Nambu, Phys. Rev. **106**, 1337 (1957).

- [4] A. I. Vainshtein and V. I. Zakharov, Nucl. Phys. B **36**, 589 (1972).  
[5] F. A. Berends, A. Donnachie, and D. L. Weaver, Nucl. Phys. B **4**, 1 (1967).  
[6] M. Hilt, B. C. Lehnardt, S. Scherer, and L. Tiator, Phys. Rev. C **88**, 055207 (2013).

- [7] C. M. G. Lattes, H. Muirhead, G. P. S. Occhialini, and C. F. Powell, *Nature* **159**, 694 (1947).
- [8] E. M. McMillan, J. M. Peterson, and R. S. White, *Science*, **110**, 579 (1949).
- [9] J. Steinberger, W. K. H. Panofsky, and J. Steller, *Phys. Rev.* **78**, 802 (1950).
- [10] C. M. G. Lattes, H. Muirhead, G. P. S. Occhialini, and C. F. Powell, *Nature*, **159**, 694 (1947).
- [11] R. S. White, M. J. Jacobson, and A. G. Schulz, *Phys. Rev.* **88**, 836 (1952).
- [12] H. L. Anderson, E. Fermi, R. Martin, and D. E. Nagle, *Phys. Rev.* **91**, no. 1, 155 (1953).
- [13] W. J. Briscoe, M. Döring, H. Haberzettl, I. I. Strakovsky, and R. L. Workman, Institute of Nuclear Studies of The George Washington University Database; <http://gwdac.phys.gwu.edu/>.
- [14] W. J. Briscoe *et al.* [A2 Collaboration], *Phys. Rev. C* **100**, no. 6, 065205 (2019).
- [15] D. Drechsel, S. S. Kamalov, and L. Tiator, *Eur. Phys. J. A* **34**, 69 (2007).
- [16] B. Strandberg *et al.* [PIONS@MAX-lab Collaboration], *Phys. Rev. C* **101**, no. 3, 035207 (2020).
- [17] J.-O. Adler *et al.*, *Nucl. Instrum. Methods Phys. Res. Sect. A* **715**, 1 (2013).
- [18] M. Eriksson, in: 5th International Particle Accelerator Conference (IPAC 2014) Proceedings, Editors: Ch. Petit-Jean-Genaz *et al.* Jun 2014. Dresden, Germany.
- [19] V. E. Tarasov, W. J. Briscoe, H. Gao, A. E. Kudryavtsev, and I. I. Strakovsky, *Phys. Rev. C* **84**, 035203 (2011).
- [20] L. D. Landau and E. M. Lifshits, “Quantum Mechanics : Non-Relativistic Theory,” (Butterworth-Heinemann, 1977).
- [21] M. I. Levchuk, A. Y. Loginov, A. A. Sidorov, V. N. Stibunov, and M. Schumacher, *Phys. Rev. C* **74**, 014004 (2006).
- [22] M. Doring, E. Oset, and M. J. Vicente Vacas, *Phys. Rev. C* **70**, 045203 (2004).
- [23] R. Machleidt, *Phys. Rev. C* **63**, 024001 (2001).
- [24] D. Drechsel and L. Tiator, *J. Phys. G* **18**, 449 (1992).
- [25] V. Lensky, V. Baru, J. Haidenbauer, C. Hanhart, A. E. Kudryavtsev, and U.-G. Meißner, *Eur. Phys. J. A* **26**, 107 (2005).
- [26] W. Chen *et al.*, *Phys. Rev. C* **86**, 015206 (2012).
- [27] W. J. Briscoe, A. E. Kudryavtsev, P. Pedroni, I. I. Strakovsky, V. E. Tarasov, and R. L. Workman, *Phys. Rev. C* **86**, 065207 (2012).
- [28] P. T. Mattione *et al.* [CLAS Collaboration], *Phys. Rev. C* **96**, no. 3, 035204 (2017).
- [29] V. Bernard, N. Kaiser, and U. G. Meißner, *Phys. Lett. B* **383**, 116 (1996).
- [30] D. H. White, R. M. Schectman, and B. M. Chasan, *Phys. Rev.* **120**, no. 2, 614 (1960).
- [31] M. Salomon, D. F. Measday, J. M. Poutissou, and B. C. Robertson, *Nucl. Phys. A* **414**, 493 (1984).
- [32] K. Liu, Ph. D. Thesis, University of Kentucky, 1994.